INTERNATIONAL JOURNAL FOR NUMERICAL METHODS IN BIOMEDICAL ENGINEERING
Int. J. Numer. Meth. Biomed. Engng. 2010; **26**:637–645
Published online 1 September 2008 in Wiley InterScience (www.interscience.wiley.com). DOI: 10.1002/cnm.1165
COMMUNICATIONS IN NUMERICAL METHODS IN ENGINEERING

Degenerate scale problem arising from curved rigid line inclusion

Y. Z. Chen*, †, X. Y. Lin and Z. X. Wang

Division of Engineering Mechanics, Jiangsu University, Zhenjiang, Jiangsu 212013, People's Republic of China

SUMMARY

This paper investigates the degenerate scale problem arising from the curved rigid line inclusion. The problem is modeled by a continuous distribution of the body force along the prospective site of the curve. In the first step, the problem is formulated on the configuration of the degenerate scale, and an integral equation is suggested. Later, after using a modification for the coordinates, the problem is solved in a modified scale or in the normal scale. From the solution of the integral equation in the normal scale, the degenerate scale will be obtained immediately. Finally, several numerical examples are given. From computed results it is proved that the degenerate scale depends only on the configuration of the curve and does not depend on the initial normal scale used. Copyright © 2008 John Wiley & Sons, Ltd.

Received 14 December 2007; Revised 19 May 2008; Accepted 8 July 2008

KEY WORDS: boundary integral equation; degenerate scale; curved rigid line inclusion; numerical solution; plane elasticity

1. INTRODUCTION

The boundary integral equation (BIE) was widely used in elasticity, and the fundamental for BIE could be found from [1–3]. Heritage and early history of the boundary element method was summarized more recently [4]. However, some difficult points for the BIE remain.

The degenerate scale problem in BIE is a particular problem in plane elasticity as well as in Laplace equation. It is typical to study the degenerate scale problem through the exterior problem of plane elasticity. Assume that there is an infinite plate with an elliptic hole. We also assume the vanishing displacements on the elliptic contour, a non-trivial solution for relevant BIE exists when a particular scale is reached. A non-trivial solution for the homogenous integral equation means that the relevant non-homogenous integral equation must have a non-unique solution. From the viewpoint of engineering, the non-unique solution is an illogical one. In the usual BIE, the homogeneous equations in the Dirichlet problem for the exterior region and the interior region are the same. Thus, the degenerate scale problem also exists in the interior problem.

The degenerate scale problem was investigated in the ring area [5, 6], plane elasticity [7–9], and Laplace equation [10]. A numerical technique for evaluating the degenerate scale was also suggested by using two sets of particular solution in the geometry of normal scale [7]. For the elliptic hole case, a closed-form solution has been obtained by using the complex variable and the elliptic coordinate [8]. From the viewpoint of linear algebra, the problem also originates from rank deficiency in the influence matrices. By using a particular solution in the normal scale, the degenerate scale can be evaluated numerically [10].

*Correspondence to: Y. Z. Chen, Division of Engineering Mechanics, Jiangsu University, Zhenjiang, Jiangsu 212013, People's Republic of China.
†E-mail: chens@ujs.edu.cn

The perspective on the degenerate problems was provided [11]. These problems include (1) the degenerate boundary, (2) the degenerate scale, (3) the spurious eigensolution, and (4) the fictitious frequency, in the boundary integral formulation. All the degenerate problems originate from the rank deficiency in the influence matrix. The current status of the formulations of the dual boundary element methods was provided [12]. In the paper, the regularizations of the hypersingular integrals and the divergent series were emphasized.

It is seen that the elliptic notch is reduced to a rigid line when the minor half-axis of the ellipse becomes zero. That is to say, the degenerate scale problem exists in the straight rigid line case. It is also easy to image that the degenerate scale problem also exists in the curved rigid line problem.

In this paper, the degenerate scale problem in the curved rigid line inclusion in plane elasticity is investigated. The problem is modeled by a continuous distribution of the body force along the prospective site of the curve. In the first step, the problem is formulated on the configuration of the degenerate scale, and an integral equation is suggested. Later, after using a modification for the used coordinates, the problem is solved in a modified scale or in the normal scale. From the solution for the integral equation in the normal scale, the degenerate scale will be obtained immediately. Finally, several numerical examples are given. It is proved from the computed results that the degenerate scale depends only on the configuration of the curve and does not depend on the initial normal scale used.

2. ANALYSIS FOR THE DEGENERATE SCALE PROBLEM ARISING FROM THE CURVED RIGID LINE INCLUSION

The complex variable function method plays an important role in plane elasticity. Fundamental of this method is introduced. In the method, the stresses $(\sigma_x, \sigma_y, \sigma_{xy})$, the resultant forces (X, Y), and the displacements (u, v) are expressed in terms of complex potentials $\phi(z)$ and $\psi(z)$ such that [13]

$$\sigma_x+\sigma_y = 4\,\mathrm{Re}\,\Phi(z)$$

$$\sigma_y-\sigma_x+2\mathrm{i}\sigma_{xy} = 2[\bar{z}\Phi'(z)+\Psi(z)] \tag{1}$$

$$f=-Y+\mathrm{i}X=\phi(z)+z\overline{\phi'(z)}+\overline{\psi(z)} \tag{2}$$

$$2G(u+\mathrm{i}v)=\kappa\phi(z)-z\overline{\phi'(z)}-\overline{\psi(z)} \tag{3}$$

where $\Phi(z)=\phi'(z)$, $\Psi(z)=\psi'(z)$, a bar over a function denotes the conjugated value for the function, G is the shear modulus of elasticity, $\kappa=(3-v)/(1+v)$ in the plane stress problem, $\kappa=3-4v$ in the plane strain problem, and v is the Poisson ratio.

Except for the physical quantities mentioned above, from Equations (2) and (3) two derivatives in the specified direction are introduced as follows [14]:

$$J_1(z)=\frac{\mathrm{d}}{\mathrm{d}z}\{-Y+\mathrm{i}X\}=\Phi(z)+\overline{\Phi(z)}+\frac{\mathrm{d}\bar{z}}{\mathrm{d}z}(z\overline{\Phi'(z)}+\overline{\Psi(z)})=N+\mathrm{i}T \tag{4}$$

$$J_2(z)=2G\frac{\mathrm{d}}{\mathrm{d}z}\{u+\mathrm{i}v\}=\kappa\Phi(z)-\overline{\Phi(z)}-\frac{\mathrm{d}\bar{z}}{\mathrm{d}z}(z\overline{\Phi'(z)}+\overline{\Psi(z)})=(\kappa+1)\Phi(z)-J_1 \tag{5}$$

It is easy to verify that $J_1=N+\mathrm{i}T$ denotes the normal and tangential tractions along the segment $\overline{z, z+\mathrm{d}z}$ (Figure 1). Secondly, the J_1 and J_2 values depend not only on the position of the point 'z', but also on the direction of the segment '$\mathrm{d}\bar{z}/\mathrm{d}z$'.

Formulation of the integral equation for the degenerate scale problem in the case of the curved rigid line is introduced below. If the concentrated forces (P_x, P_y) is applied at the point $z=t$ (Figure 1(a)), the relevant complex potentials are defined as [13]

$$\phi(z)=F\ln(z-t), \quad \psi(z)=-\kappa\bar{F}\ln(z-t)-\frac{F\bar{t}}{z-t} \tag{6}$$

DOI: 10.1002/cnm

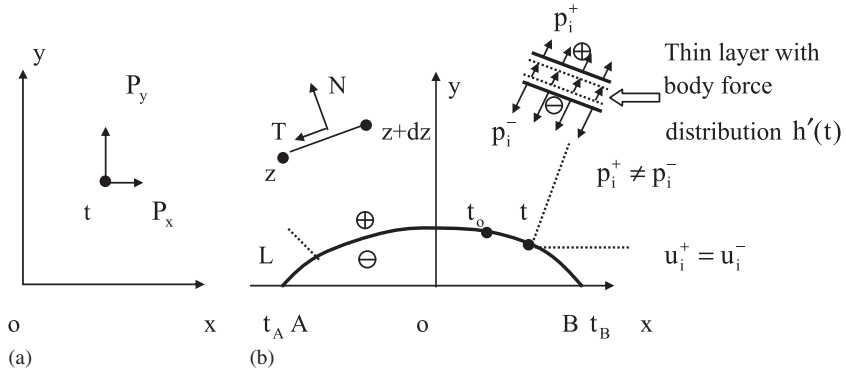

Figure 1. (a) A pair of concentrated forces (P_x, P_y) applied at the point $z=t$ and (b) a curved rigid line with distributed body force.

where

$$F=-\frac{P_x+\mathrm{i}P_y}{2\pi(\kappa+1)} \tag{7}$$

After letting $F=-h'(t)\,\mathrm{d}t/2\pi$ $(h'(t)=\mathrm{d}h(t)/\mathrm{d}t)$ and taking integration along the curve L (Figure 1(b)), we will obtain the following complex potentials [15]:

$$\phi(z)=-\frac{1}{2\pi}\int_L \ln(z-t)h'(t)\,\mathrm{d}t,\quad \phi'(z)=\frac{1}{2\pi}\int_L \frac{h'(t)\,\mathrm{d}t}{t-z},\quad \phi''(z)=\frac{1}{2\pi}\int_L \frac{h'(t)\,\mathrm{d}t}{(t-z)^2} \tag{8}$$

$$\psi(z)=\frac{\kappa}{2\pi}\int_L \ln(z-t)\overline{h'(t)}\,\mathrm{d}\bar{t}-\frac{1}{2\pi}\int_L \frac{\bar{t}h'(t)\,\mathrm{d}t}{t-z}$$

$$\psi'(z)=-\frac{\kappa}{2\pi}\int_L \frac{\overline{h'(t)}\,\mathrm{d}\bar{t}}{t-z}-\frac{1}{2\pi}\int_L \frac{\bar{t}h'(t)\,\mathrm{d}t}{(t-z)^2} \tag{9}$$

Substituting Equations (8) and (9) into Equations (2) and (3) yields

$$2G(u(z)+\mathrm{i}v(z))=-\frac{\kappa}{2\pi}\int_L (\ln(t-z)+\overline{\ln(t-z)})h'(t)\,\mathrm{d}t+\frac{1}{2\pi}\int_L \frac{(t-z)\overline{h'(t)}\,\mathrm{d}\bar{t}}{\bar{t}-\bar{z}} \tag{10}$$

$$f(z)=(\kappa+1)\phi(z)-2G(u(z)+\mathrm{i}v(z)) \tag{11}$$

The contour increment for some functions plays an important role in the analysis. When a point 'z' is going around a large circle in an anti-clockwise direction, the increment of a function, say $\phi(z)$, is defined as $\{\phi(z)\}_{\mathrm{in}}$. From this definition and Equations (2), (3), (8), and (9), we have

$$\{\phi(z)\}_{\mathrm{in}}=-\mathrm{i}\int_L h'(t)\,\mathrm{d}t,\quad \{\psi(z)\}_{\mathrm{in}}=\kappa\mathrm{i}\int_L \overline{h'(t)}\,\mathrm{d}\bar{t} \tag{12}$$

$$\{f\}_{\mathrm{in}}=-\mathrm{i}(\kappa+1)\int_L h'(t)\,\mathrm{d}t,\quad \{2G(u+\mathrm{i}v)\}_{\mathrm{in}}=0 \tag{13}$$

The first part of Equation (13) reveals that there may be some loadings applied on the curved rigid line. The second part of Equation (13) reveals that the single-valued condition of the displacements is satisfied automatically.

Letting $z\to t_0^+$ or $z\to t_0^-$ (Figure 1(b)), in either case from Equation (10) we will find

$$2G(u(t_0)+\mathrm{i}v(t_0))^{\pm}=-\frac{\kappa}{\pi}\int_L \ln|t-t_0|h'(t)\,\mathrm{d}t+\frac{1}{2\pi}\int_L \frac{(t-t_0)\overline{h'(t)}\,\mathrm{d}\bar{t}}{\bar{t}-\bar{t}_0} \tag{14}$$

DOI: 10.1002/cnm

In what follows, we define the jump value for a function $\phi(z)$ along a curve by $\{\phi(t)\}_j = \phi^+(t) - \phi^-(t)$ $(t \in L)$, where $\phi^+(t)$ (or $\phi^-(t)$) denotes the limit value of $\phi(z)$ from upper side $z \to t^+$ (or lower side $z \to t^-$), respectively. From the property of the logarithmic function and Equation (8) we find

$$\{\phi(t_0)\}_j = \mathrm{i}h(t_0) \quad (t_0 \in L) \tag{15}$$

where

$$h(t_0) = \int_{t_A}^{t_0} h'(t)\,\mathrm{d}t \quad (t_0 \in L) \tag{16}$$

In addition, from Equation (14) we find

$$2G(u(t_0) + \mathrm{i}v(t_0))_j = 0 \quad (t_0 \in L) \tag{17}$$

Further, from Equations (11), (15), and (17), we have

$$(-\mathrm{i}f(t_0))_j = (X(t_0) + \mathrm{i}Y(t_0))_j = (\kappa+1)h(t_0) \quad (t_0 \in L) \tag{18}$$

From Equations (17) and (18), we see that the displacements are continuous when a point is moving across the curved line, and the resultant forces are discontinuous in the same condition. From Equation (18) it follows that

$$h'(t_0) = \frac{1}{\kappa+1}\frac{\mathrm{d}\{-\mathrm{i}f(t_0)\}_j}{\mathrm{d}t_0} = -\frac{\mathrm{i}\{J_1(t_0)\}_j}{\kappa+1} \quad (t_0 \in L) \tag{19}$$

Equation (19) reveals that there is a body force distribution along the curve L (Figure 1(b)). Alternatively, the following properties $u_i^+ = u_i^-$ and $p_i^+ \neq p_i^-$ hold along the curve L.

As in the usual BIE for the exterior problem, we can impose the following condition in the degenerate scale problem of the curved rigid line:

$$(u(t_0) + \mathrm{i}v(t_0))^{\pm} = 0 \quad (t_0 \in L) \tag{20}$$

Thus, from Equations (14) and (20), we will find the following integral equation for the degenerate scale problem:

$$2\kappa \int_L \ln|t - t_0| h'(t)\,\mathrm{d}t - \int_L \frac{(t - t_0)\overline{h'(t)}\,\mathrm{d}\bar{t}}{\bar{t} - \bar{t}_0} = 0 \tag{21}$$

In conclusion, a particular size for the curved rigid line is sought under the condition that Equation (21) has a non-trivial solution ($h'(t) \neq 0$). Therefore, it is preferable to catalog the studied problem in the range of the degenerate scale problem. Alternatively, in the curved rigid line case there is also a degenerate scale problem.

The solution technique for the integral equation for the degenerate scale problem is introduced below. Without loss of the generality, the problem is solved for a parabolic configuration (Figure 2):

$$y = \delta a\left(1 - \frac{x^2}{a^2}\right) \quad (\delta\text{-constant}, |x| \leqslant a) \tag{22}$$

In the first step, Equation (21) is formulated on the degenerate scale using the coordinates $o_* x_* y_*$ (Figure 2(a)). In this case, Equation (21) can be rewritten as

$$2\kappa \int_{L_d} \ln|t - t_0| h'(t)\,\mathrm{d}t - \int_{L_d} \frac{(t - t_0)\overline{h'(t)}\,\mathrm{d}\bar{t}}{\bar{t} - \bar{t}_0} = 0 \quad (\text{in the coordinates } o_* x_* y_*) \tag{23}$$

In Equation (23), the integration is performed on the curve L_d in the coordinates $o_* x_* y_*$ (Figure 2(a)).

DOI: 10.1002/cnm

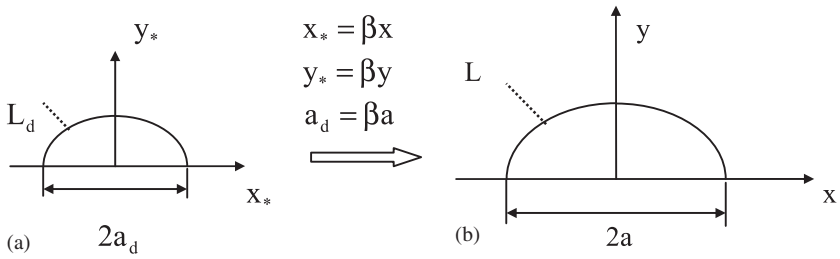

Figure 2. (a) A parabolic rigid line in a degenerate scale and (b) a parabolic rigid line in a normal scale.

Similar to the degenerate scale problem in plane elasticity or in Laplace equation [7, 8, 10], one may introduce a transform of coordinates as follows (Figure 2):

$$x_* = \beta x, \quad y_* = \beta y \tag{24}$$

Simply because $\ln|t-t_0|_{\text{in } o_*x_*y_*} = \ln|t-t_0|_{\text{in } oxy} + \ln\beta$, substituting Equation (24) into (23) yields

$$2\kappa \int_L \ln|t-t_0|\, h'(t)\,\mathrm{d}t - \int_L \frac{(t-t_0)\overline{h'(t)}\,\mathrm{d}\bar{t}}{\bar{t}-\bar{t}_0} = \frac{1}{\gamma}\int_L h'(t)\,\mathrm{d}t \quad \text{(in the coordinates } oxy) \tag{25}$$

where

$$\frac{1}{\gamma} = -2\kappa \ln\beta \tag{26}$$

In Equation (25), the integration is performed on the curve in the coordinates oxy (Figure 2(b)).

Let

$$\int_L h'(t)\,\mathrm{d}t = c_1 + \mathrm{i}c_2 \tag{27}$$

Equation (25) can be rewritten as

$$2\kappa \int_L \ln|t-t_0|\, h'(t)\,\mathrm{d}t - \int_L \frac{(t-t_0)\overline{h'(t)}\,\mathrm{d}\bar{t}}{\bar{t}-\bar{t}_0} = \frac{1}{\gamma}(c_1 + \mathrm{i}c_2) \quad \text{(in the coordinates } oxy) \tag{28}$$

It is assumed that the configuration in the coordinates oxy is in a normal scale. Thus, from Equation (28) we have a definite solution for $h'(t)$.

On the other hand, one may introduce two fundamental solutions. When a particular function is assumed in the right-hand term of Equation (28), the relevant solution for the density function $h'(t)$ is called the fundamental solution.

If the right-hand term in Equation (28) is changed by 1 and $h'(t)$ by $h_1'(t)$, we have

$$2\kappa \int_L \ln|t-t_0|\, h_1'(t)\,\mathrm{d}t - \int_L \frac{(t-t_0)\overline{h_1'(t)}\,\mathrm{d}\bar{t}}{\bar{t}-\bar{t}_0} = 1 \quad \text{(in the coordinates } oxy) \tag{29}$$

The solution from integral equation (29), or $h_1'(t)$, is called the first fundamental solution. The relevant resultant force is expressed as

$$\int_L h_1'(t)\,\mathrm{d}t = b_{11} + \mathrm{i}b_{12} \tag{30}$$

Similarly, if the right-hand term in Equation (28) is changed by i and $h'(t)$ by $h_2'(t)$, we have

$$2\kappa \int_L \ln|t-t_0|\, h_2'(t)\,\mathrm{d}t - \int_L \frac{(t-t_0)\overline{h_2'(t)}\,\mathrm{d}\bar{t}}{\bar{t}-\bar{t}_0} = i \quad \text{(in the coordinates } oxy) \tag{31}$$

DOI: 10.1002/cnm

The solution from integral equation (31), or $h_2'(t)$, is called the second fundamental solution. The relevant resultant force is expressed as

$$\int_L h_2'(t)\,\mathrm{d}t = b_{21} + \mathrm{i}b_{22} \tag{32}$$

From Equations (28), (29), and (31), we see that the investigated density function $h'(t)$ can be expressed through two fundamental solutions, which is as follows:

$$h'(t) = \frac{1}{\gamma}(c_1 h_1'(t) + c_2 h_2'(t)) \tag{32a}$$

Simply because the solution of Equation (28) (or $h'(t)$) is a linear superposition of the two fundamental solutions (or $h_1'(t), h_2'(t)$), from Equations (27) to (32) we obtain

$$\frac{c_1}{\gamma}(b_{11} + \mathrm{i}b_{12}) + \frac{c_2}{\gamma}(b_{21} + \mathrm{i}b_{22}) = c_1 + \mathrm{i}c_2 \tag{33}$$

From the condition that c_1 and c_2 have a non-trivial solution, from Equation (33) we have

$$(\gamma - b_{11})(\gamma - b_{22}) - b_{12}b_{21} = 0 \tag{34}$$

Generally, Equation (34) has two roots $\gamma = \gamma_1$ and $\gamma = \gamma_2$. Once the value γ is evaluated, from Equation (26) we can obtain

$$\beta = \exp\left(-\frac{1}{2\gamma\kappa}\right) \tag{35}$$

Finally, the degenerate scale, for example, is obtained as follows (Figure 2):

$$a_d = \beta a \tag{36}$$

3. NUMERICAL SOLUTION AND EXAMPLES

In the numerical solution, the curve is divided into N divisions, from $\overline{p_1 p_2}$, $\overline{p_2 p_3}, \ldots, \overline{p_j p_{j+1}}, \ldots, \overline{p_N p_{N+1}}$ (Figure 3). In computation $N = 120$ is used. The observation points t_0 in Equations (25), (28), (29), or (31) are assumed at the middle point of divisions and are denoted by $q_1, q_2, \ldots, q_{\mathrm{N}}$. Simply because of singular behavior for the function $h'(t)$ at the rigid line tip, on the first division we can assume

$$h'(t)|_{t=t(s_1)} = (c_1 + d_1)\sqrt{\frac{2s_1}{h_1 + s_1}} \quad (\text{for } |s_1| < h_1 \text{ along division } \overline{p_1 p_2}) \tag{37}$$

The similar expression is used for the last division $\overline{p_N p_{N+1}}$. For the intermediate divisions, it is assumed that

$$h'(t)|_{t=t(s_j)} = (c_j + \mathrm{i}d_j) \quad (\text{along the divisions } \overline{p_j p_{j+1}},\ j = 2, 3, \ldots, N-1) \tag{38}$$

The following integration is useful in the numerical solution:

$$\int_{-d}^{d} \frac{\sqrt{2d}\ln|s|}{\sqrt{d+s}}\,\mathrm{d}s = 4\sqrt{2}d\{\sqrt{2}(\ln b - 1) + \ln(1+\sqrt{2})\} \quad \text{with } d = b^2 \tag{39}$$

Therefore, after discretization for Equations (25), (28) (29), or (31), those integral equations can be solved numerically with the unknowns c_j, d_j $(j = 1, 2, \ldots, N)$. After the algebraic equation for c_j, d_j $(j = 1, 2, \ldots, N)$ is solved, other computations are straightforward. Three numerical examples are presented below.

DOI: 10.1002/cnm

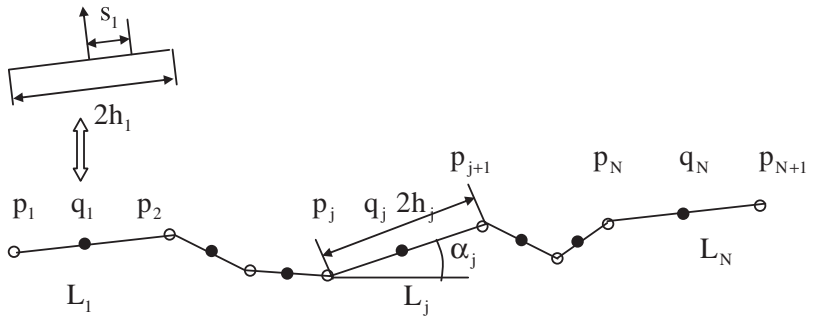

Figure 3. Discretization in the numerical solution of integral equation for the curved rigid line.

Table I. Degenerate scales $a_{d1}=f_1(\delta)$ and $a_{d2}=f_2(\delta)$ for a parabolic curve rigid line when using different initial normal scales for the dimension 'a' ($a=1$, 10, and 20) (see Equation (40) and Figure 2).

δ	0	0.1	0.2	0.3	0.4	0.5	0.6	0.7	0.8	0.9	1.0
Using the initial normal scale $a=1$											
$f_1(\delta)$	2.64094	2.60975	2.52438	2.40400	2.26836	2.13161	2.00161	1.88170	1.77269	1.67414	1.58514
$f_2(\delta)$	1.51505	1.51353	1.50875	1.50028	1.48788	1.47172	1.45226	1.43013	1.40598	1.38042	1.35395
Using the initial normal scale $a=10$											
$f_1(\delta)$	2.63953	2.60835	2.52304	2.40273	2.26716	2.13049	2.00056	1.88072	1.77176	1.67326	1.58431
$f_2(\delta)$	1.51424	1.51273	1.50795	1.49948	1.48709	1.47093	1.45148	1.42937	1.40524	1.37969	1.35323
Using the initial normal scale $a=20$											
$f_1(\delta)$	2.63910	2.60793	2.52264	2.40234	2.26680	2.13015	2.00024	1.88042	1.77148	1.67300	1.58406
$f_2(\delta)$	1.51400	1.51248	1.50771	1.49924	1.48685	1.47070	1.45125	1.42914	1.40501	1.37947	1.35302

Example 3.1: In the first example, the curved rigid line has the configuration shown by Equation (22). As mentioned previously, there are two degenerate scales. Those degenerate scales are expressed as

$$a_{d1}=f_1(\delta), \quad a_{d2}=f_2(\delta) \tag{40}$$

Three cases, $a=1$, 10, and 20, for the normal scale are chosen in computation. The relevant computed results for $f_1(\delta)$ and $f_2(\delta)$ for $\delta=0, 0.1, 0.2, \ldots, 1.0$ are listed in Table I. From the tabulated results, we see that the final computed results for the degenerate scale do not depend on the initial input value for the normal scale ($a=1$, 10, and 20). In addition, for $\delta=0$ case, or for a straight rigid line, the relevant degenerate scales are $a_{d1}=2\exp(1/2\kappa)=2.64039$ and $a_{d2}=2\exp(-1/2\kappa)=1.51493$ (using $\kappa=1.8$) [8]. From Table I, we see that the computed results are sufficiently accurate.

Example 3.2: In the second example, an arc rigid line is under consideration (Figure 4(a)). As mentioned previously, there are two degenerate scales. Those degenerate scales are expressed in two forms

$$R_{d1}=f_1(\beta), \quad R_{d2}=f_2(\beta) \tag{41}$$

or

$$\beta R_{d1}=\beta f_1(\beta)=g_1(\beta), \quad \beta R_{d2}=\beta f_2(\beta)=g_2(\beta) \tag{42}$$

In computation, we choose the normal scale $R=0.5$; the relevant computed results for $f_1(\beta)$ and $f_2(\beta)$ and $g_1(\beta)$ and $g_2(\beta)$ for $\beta=\pi/12, 2\pi/12, \ldots, 11\pi/12$ are listed in Table II. In addition, for $\beta=\pi/12$ case, the arc crack has a slight difference with a line rigid line, and we have $g_1(\beta)|_{\beta=\pi/12}=2.61840$, $g_2(\beta)|_{\beta=\pi/12}=1.53051$. This result is close to that for the straight rigid

DOI: 10.1002/cnm

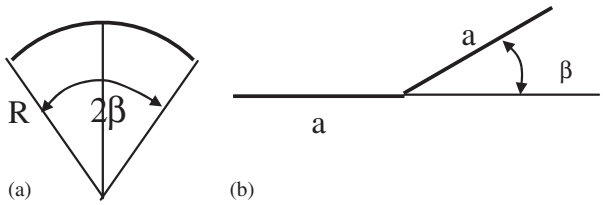

Figure 4. (a) An arc rigid line in a normal scale and (b) a kinked rigid line in a normal scale.

Table II. Degenerate scales $R_{d1}=f_1(\beta)$, $R_{d2}=f_2(\beta)$, $\beta R_{d1}=g_1(\beta)$, $\beta R_{d2}=g_2(\beta)$ for an arc rigid line (see Equations (41) and (42) and Figure 4(a)).

β	$\pi/12$	$2\pi/12$	$3\pi/12$	$4\pi/12$	$5\pi/12$	$6\pi/12$	$7\pi/12$	$8\pi/12$	$9/12$	$10\pi/12$	$11\pi/12$
$f_1(\beta)$	10.0016	4.88068	3.15230	2.29496	1.80023	1.49365	1.29698	1.16927	1.08710	1.03647	1.00905
$f_2(\beta)$	5.84613	3.00680	2.09714	1.66859	1.43050	1.28490	1.18898	1.12117	1.07054	1.03295	1.00882
$g_1(\beta)$	2.61840	2.55552	2.47581	2.40328	2.35650	2.34622	2.37684	2.44892	2.56142	2.71346	2.90585
$g_2(\beta)$	1.53051	1.57435	1.64709	1.74735	1.87251	2.01832	2.17893	2.34817	2.52239	2.70426	2.90520

Table III. Degenerate scales $a_{d1}=f_1(\beta)$ and $a_{d2}=f_2(\beta)$ for a kinked rigid line (see Equation (43) and Figure 4(b)).

β	0	$\pi/12$	$2\pi/12$	$3\pi/12$	$4\pi/12$	$5\pi/12$	$6\pi/12$	$7\pi/12$	$8\pi/12$	$9/12$	$10\pi/12$
$f_1(\beta)$	2.64094	2.63133	2.60444	2.56563	2.52250	2.48358	2.45737	2.45206	2.50085	2.87789	3.39206
$f_2(\beta)$	1.51505	1.52657	1.56172	1.62237	1.71184	1.83519	1.99982	2.21643	2.47599	2.53874	2.65453

line case, or the case of $\delta=0$ in Example 3.1, where the relevant degenerate scales are 2.64039 and 1.51493, respectively.

Example 3.3: In the third example, the curved rigid line has the kinked configuration with a kinked angle from $\beta=0$, $\pi/12$, $2\pi/12$ $3\pi/12,\ldots,10\pi/12$ (Figure 4(b)). As before, the computed degenerate scales are expressed as

$$a_{d1}=f_1(\beta),\quad a_{d2}=f_2(\beta) \tag{43}$$

In computation, we choose the normal scale $a=1$. The relevant computed results for $f_1(\beta)$ and $f_2(\beta)$ for $\beta=0$, $\pi/12$, $2\pi/12$, $3\pi/12,\ldots,10\pi/12$ are tabulated in Table III.

4. CONCLUSIONS

In order to solve the degenerate scale problem, the relevant integral equation is solved in the normal scale [7, 10]. This technique is also efficient in the degenerate scale problem of the curved rigid line. Researchers may concern about how to choose the normal scale in computation. This problem is easy to deal with. In fact, after the Fortran program is completed, one can input some initial normal scale, for example, $a=0.8$ in Example 3.1. If we do not satisfy the results from computation, we simply change the input value for 'a', for example, $a=1$, 10, and 20 in Example 3.1. The computation is finished once the computed results for a_{d1} and a_{d2} have a large difference from the input value of 'a'. It was found that one set of computation takes only 15 s in all examples cited previously.

REFERENCES

1. Rizzo FJ. An integral equation approach to boundary value problems in classical elastostatics. *Quarterly Journal of Applied Mathematics* 1967; **25**:83–95.

DOI: 10.1002/cnm

2. Cruse TA. Numerical solutions in three-dimensional elastostatics. *International Journal of Solids and Structures* 1969; **5**:1259–1274.
3. Brebbia CA, Tells JCF, Wrobel LC. *Boundary Element Techniques—Theory and Application in Engineering*. Springer: Heidelberg, 1984.
4. Cheng AHD, Cheng DS. Heritage and early history of the boundary element method. *Engineering Analysis with Boundary Elements* 2005; **29**:286–302.
5. He WJ, Ding HJ, Hu HC. Degenerate scales and boundary element analysis of two dimensional potential and elasticity problems. *Computers and Structures* 1996; **60**:155–158.
6. Chen YZ, Wang ZX, Lin XY. Numerical examination for degenerate scale problem for ellipse-shaped region in BIE. *International Journal for Numerical Methods in Engineering* 2007; **71**:1208–1220.
7. Vodička R, Mantič V. On solvability of a boundary integral equation of the first kind for Dirichlet boundary value problems in plane elasticity. *Computational Mechanics* 2007; DOI: 10.1007//s00466-007-0202-x.
8. Chen JT, Kuo SR, Lin JH. Analytical study and numerical experiments for degenerate scale problems in the boundary element method of two-dimensional elasticity. *International Journal for Numerical Methods in Engineering* 2002; **54**:1669–1681.
9. Vodička R, Mantič V. On invertibility of elastic single-layer potential operator. *Journal of Elasticity* 2004; **74**:147–173.
10. Chen JT, Lin SR, Chen KH. Degenerate scale problem when solving Laplace's equation by BEM and its treatment. *International Journal for Numerical Methods in Engineering* 2005; **62**:233–261.
11. Chen JT, Lin SR. On the rank-deficiency problems in the boundary integral formulation using the Fredholem alternative theorem and singular value decomposition technique. *Fifth World Congress on Computational Mechanics*, Vienna, Austria, 2002.
12. Chen JT, Hong HK. Review of dual boundary element methods with emphasis on hypersigular integrals and divergent series. *Applied Mechanics Review* 1999; **52**:17–33.
13. Muskhelishvili NI. *Some Basic Problems of Mathematical Theory of Elasticity*. Noordhoof: The Netherlands, 1953.
14. Chen YZ, Hasebe N, Lee KY. *Multiple Crack Problems in Elasticity*. WIT Press: Southampton, 2003.
15. Chen YZ, Lin XY. Complex potentials and integral equations for curved crack and curved rigid line problems in plane elasticity. *Acta Mechanica* 2006; **182**:211–230.

DOI: 10.1002/cnm